



HAL
open science

Single star scidar: atmospheric parameters profiling using the simulated annealing algorithm

A. Habib, J. Vernin, Z. Benkhaldoun, H. Lanteri

► **To cite this version:**

A. Habib, J. Vernin, Z. Benkhaldoun, H. Lanteri. Single star scidar: atmospheric parameters profiling using the simulated annealing algorithm. *Monthly Notices of the Royal Astronomical Society*, 2006, 368, pp.1456-1462. hal-00416992

HAL Id: hal-00416992

<https://hal.science/hal-00416992>

Submitted on 17 Jun 2021

HAL is a multi-disciplinary open access archive for the deposit and dissemination of scientific research documents, whether they are published or not. The documents may come from teaching and research institutions in France or abroad, or from public or private research centers.

L'archive ouverte pluridisciplinaire **HAL**, est destinée au dépôt et à la diffusion de documents scientifiques de niveau recherche, publiés ou non, émanant des établissements d'enseignement et de recherche français ou étrangers, des laboratoires publics ou privés.

Single star scidar: atmospheric parameters profiling using the simulated annealing algorithm

A. Habib,¹ J. Vernin,^{2*} Z. Benkhaldoun¹ and H. Lanteri²

¹*UFR : APHE, Université Cadi Ayyad, Faculté des Sciences Semlalia, Av. Prince My Abdellah, BP 2390 Marrakech, Morocco*

²*L.U.A.N CNRS/UMR 6525 – Université de Nice-Sophia Antipolis, 06108 Nice Cedex 2, France*

Accepted 2006 February 22. Received 2005 December 28

ABSTRACT

In this paper, we present a new method to estimate, for each turbulent layer labelled i , the horizontal wind speed $v(h_i)$, the standard deviation of the horizontal wind speed fluctuations $\sigma_v(h_i)$ and the integrated value of C_n^2 over the thickness Δh_i of the turbulent layer $C_n^2(h_i)\Delta h_i$, where h_i is the altitude of the turbulent layer. These parameters are extracted from single star scintillation spatiotemporal cross-correlation functions of atmospheric speckles obtained within the generalized mode. This method is based on the simulated annealing algorithm to find the optimal solution required to solve the problem. Astrophysics parameters for adaptive optics are also calculated using $C_n^2(h_i)$ and $v(h_i)$ values. The results of other techniques support this new method.

Key words: turbulence – atmospheric effects – balloons – methods: data analysis – methods: statistical – site testing.

1 INTRODUCTION

The analysis of stellar scintillation enables us to obtain information about the optical quality of the atmosphere. Optical remote sensing of atmospheric turbulence allows us to obtain the vertical profiles of turbulence strength $C_n^2(h)$, the wind speed $v(h)$ and the standard deviation of the horizontal wind speed fluctuations $\sigma_v(h)$.

Tatarski (1961) and Roddier (1981) developed the mathematical formulae to describe the scintillation phenomena. Vernin & Roddier (1973) and Rocca, Roddier & Vernin (1974) settled the basis of the multidimensional analysis of the stellar scintillation in order to separate the effect of each optical turbulent layer.

Caccia, Azouit & Vernin (1987) and Caccia & Vernin (1990) demonstrated that optical turbulence and wind speed profiles can be obtained with single star scintillation analysis if one takes into account the dispersion of wind speed fluctuations σ_v . This variable accounts for the spreading and the attenuation of the spatiotemporal cross-correlation peaks (see Section 2). However, it requires the calculation of a great number of spatiotemporal cross-correlation functions for various temporal delays. Habib, Vernin & Benkhaldoun (2005) introduced a simple method to find atmospheric parameters, using single star scintillation, in the Fourier domain. This method requires only the calculation of two spatiotemporal cross-correlations between atmospheric speckles (scintillation images) present in the analysis plane and delayed by τ_1 and τ_2 . But, the Fourier method is inapplicable when correlation peaks are not well separated, which

occurs when wind speeds are close or when temporal delays are small.

In this paper, we will introduce a new technique in order to retrieve the atmospheric parameters by the analysis of a single star scintillation even if the correlation peaks are mixed. This method is based on the simulated annealing (SA) principle to find the optimal solution to the problem.

2 BRIEF REVIEW

The goal of the single star scidar (SSS) technique is the determination, for each turbulent layer of altitude h_i , of the horizontal wind speed $v(h_i)$, the standard deviation of horizontal wind speed fluctuations $\sigma_v(h_i)$ and the integrated value $C_n^2(h_i)\Delta h_i$ of C_n^2 over the thickness Δh_i of the turbulent layer. This study makes it possible to extract these atmospheric parameters from spatiotemporal cross-correlation functions of atmospheric speckles $C(\mathbf{r}, \tau)$ taken at the moment t in \mathbf{r}_0 and this same speckle taken at moment $t + \tau$ in $\mathbf{r}_0 + \mathbf{r}$. This function is written as:

$$C(\mathbf{r}, \tau) = \sum_{i=1}^N C(\mathbf{r}, h_i) * G(\mathbf{r}, \sigma_{v_i} \tau) * S(\mathbf{r}) * \delta(\mathbf{r} - v_i \tau) + n(\mathbf{r}), \quad (1)$$

where:

- (i) $*$ denotes a convolution product;
- (ii) \mathbf{r} is the position vector in the 2D correlation plane;
- (iii) τ is the laps-time between two scintillation images;
- (iv) N is the number of sampling steps of ‘ h ’;
- (v) h_i is the altitude of the turbulent layer i ;

*E-mail: vernin@unice.fr

(vi) $C(\mathbf{r}, h_i)$ is the spatial auto-correlation function of the scintillation image corresponding to the turbulent layer i . The Fourier transformation (FT) of this function is the power spectrum of the scintillation $W(\mathbf{f}, h_i) = \text{FT}[C(\mathbf{r}, h_i)]$, which is expressed by the equation (Vernin & Azouit 1983a):

$$W(\mathbf{f}, h_i) = 1.54\lambda^{-2}|\mathbf{f}|^{-(11/3)}C_n^2(h_i)\Delta h_i \sin^2(\pi\lambda h_i f^2), \quad (2)$$

where \mathbf{f} is the horizontal spatial frequency vector, λ is the wavelength of the light and $C_n^2(h_i)\Delta h_i$ is the integral of $C_n^2(h)$ over the thickness of the turbulent layer. This equation is valid under the approximation of small perturbations. It has been shown (Vernin & Azouit 1983a) that this hypothesis is verified when we observe stars close to the zenith;

(vii) $\delta(\mathbf{r} - \mathbf{v}_i\tau)$ introduces the horizontal movement, at speed \mathbf{v}_i , of the turbulent layer i . Rocca et al. (1974) employed Taylor's hypothesis to show that atmospheric speckle corresponding to the turbulent layer i moves at the same speed \mathbf{v}_i without distortion during the laps-time τ ;

(viii) $S(\mathbf{r})$ introduces the impulse response of the camera;

(ix) $G(\mathbf{r}, \sigma_v, \tau)$ is a Gaussian function which introduces the standard deviation of horizontal wind fluctuations (σ_v). It spreads and attenuates the spatiotemporal cross-correlation peaks. This Gaussian model supposes that there are not significant intermittencies or waves perturbing the turbulent regime during the integration time (Caccia & Vernin 1990);

(x) $n(\mathbf{r})$ is the noise term assumed to be an additive Gaussian with zero mean.

The function $C(\mathbf{r}, \tau)$ satisfies Taylor's hypothesis and the Gaussian model of wind speed fluctuations and contains all the atmospheric parameters we are looking for. Since, it is difficult to detect the difference between a low-altitude peak spread by a large σ_v Gaussian function and a high-altitude peak spread by a small σ_v Gaussian function (Caccia & Vernin 1990), we should use at least two spatiotemporal cross-correlation functions to avoid this ambiguity.

One needs to fit the experimental results of the left-hand side of equation (1) with the sum of theoretical functions which depend on parameters we want to assess [$C_n^2(h_i)$, $v_x(h_i)$, $v_y(h_i)$, $\sigma_v(h_i)$]. To find these parameters, we need to minimize the following function:

$$E = \sum_i [C(\mathbf{r}_i, \tau) - C_{\text{th}}(\mathbf{r}_i, \tau)]^2, \quad (3)$$

$C(\mathbf{r}, \tau)$ being the experimental spatiotemporal cross-correlation of the scintillation and $C_{\text{th}}(\mathbf{r}, \tau)$ the theoretical spatiotemporal cross-correlation corresponding to a given solution.

Since each turbulent layer, at altitude h , is characterized by four parameters, a configuration (solution) is a combination of four N parameters. From experimental tests, it appeared that this function is non-convex and classical local minimization methods are to no avail and could lead to local minima. That is why we used the SA method, which is a global minimization method.

3 THE PRINCIPLE OF THE SIMULATED ANNEALING METHOD

3.1 Introduction

The SA method is a probabilistic algorithm for a global optimization problem. It is based on Metropolis criterion and was introduced by Kirkpatrick, Gelett & Vecchi (1983). The name comes from annealing in metallurgy. Let us consider a substance in thermodynamic

equilibrium at temperature T . The probability $\mathcal{P}(E)$ of this state of energy E is given by Boltzman law: $\mathcal{P}(E) = \exp(-E/K_B T)$, K_B is the Boltzman constant. If we decrease the temperature slowly, this system will reach another thermodynamic equilibrium state. If we repeat this process until zero temperature, we can obtain a perfect crystal with a lower energy.

The SA is a numerical simulation of the metallurgical annealing process where controlled cooling is used in order to create a crystal with a lower internal energy.

3.2 Simulated annealing algorithm

The research of the configuration which minimizes the cost function E (analogue of internal energy) goes through the following stages as follows.

(i) Initially, we choose the initial value T_0 of the control parameter T (analogue of temperature).

(ii) We start with any configuration of the atmospheric parameters. Let us consider E as the corresponding cost function.

(iii) We randomly carry out a disturbance to the system state. This means that we randomly choose one of the four N parameters, then we randomly modify it by adding or subtracting some small amount. Consequently, the system cost function becomes E' .

(iv) Acceptance test:

– If the difference $\delta E = E' - E$ is negative, we accept the new configuration.

– If the new cost function (E') is higher than the previous one (E), the new configuration may be accepted with probability $\mathcal{P} = \exp(-\delta E/T)$, that is, if the probability \mathcal{P} is larger than a uniformly selected random number between 0 and 1, the new configuration is accepted, if not, we keep to the previous configuration. This is called the Metropolis criterion.

We should note that the Metropolis criterion prevents the algorithm from getting stuck in local minima.

(v) We repeat the stages (iii) and (iv) until the cost function reaches a stationary value.

(vi) Once the stationary state (analogue of thermodynamics equilibrium state) is reached, we slightly decrease the parameter T , that is, we multiply T by a numerical factor of α ($\alpha < 1$).

Then, we repeat stages (iii), (iv) and (v).

(vii) The algorithm is stopped when the cost function becomes almost equal to the cost function E_n of the noise term $n(\mathbf{r})$ which is defined as:

$$E_n = \sum_i [n(\mathbf{r}_i)]^2. \quad (4)$$

At this stage, the decrease in the parameter T becomes ineffective.

Remark: to calculate the initial value T_0 of the control parameter we carry out a certain number (100 for example) of iterations (stages iii and iv) at a given value T and calculate the rate of acceptance, that is, the ratio of the number of accepted configurations that increase the cost function and the total number of configurations that increase the cost function. If this rate is higher than 0.8, T is accepted as an initial value, if not, we double it and start the process again.

4 EXPERIMENTAL RESULTS

4.1 Observing campaign

The experiment was performed with a 152-cm telescope at the Observatoire de Haute Provence (OHP) between 2004 November 22

and December 4. The altitude of the observatory is 650-m above the sea level. We observed the single star was β Tauri (mag = 1.7). The analysis plane was situated 1-km below the telescope pupil ($h_{\text{sg}} = -1$ km). The exposure time of each image was 1 ms and the minimal time-lapse between two images was 5.6 ms. A set of six spatiotemporal cross-correlation functions (see Fig. 1) was recorded every 11.2 s which corresponds to a set of 2000 images. From our optical and CCD combination, the pixel size is 2-cm projected on the pupil plane. Along with the SSS measurements, we launched several instrumented balloons equipped with microthermal sensors which allow us to retrieve simultaneous optical turbulence and wind speed profiles (Azouit & Vernin 2005).

4.2 Data reduction

The results we are going to present correspond to the single star β Tauri on the night of 2004 November 23 from 23h58 UT. Fig. 1 shows the spatiotemporal cross-correlation functions ac ($\tau = 0$ ms), $ic1$ ($\tau = 11.2$ ms), $ic2$ ($\tau = 16.8$ ms), $ic3$ ($\tau = 22.4$ ms), $ic4$ ($\tau = 28$ ms) and $ic5$ ($\tau = 33.6$ ms). We can see that the spatiotemporal cross-correlation peaks are well separated in $ic3$, $ic4$ and $ic5$ but are mixed in $ic1$ and $ic2$. In order to find the atmospheric parameters, we are going to use and compare two methods: first one refers to the FT technique used by Habib et al. (2005) from which we can work out the atmospheric parameters using correlations functions $ic3$, $ic4$ and $ic5$ where the correlation peaks are separated enough. The second method (SA) is the new one, with which we expect to

reduce the data even if the correlation peaks are mixed as in $ic1$ and $ic2$.

4.2.1 Results extracted from cross-correlations $ic3$, $ic4$ and $ic5$

Using the spatiotemporal cross-correlations $ic3$, $ic4$ and $ic5$, we have obtained Fig. 2, which shows the average, from 23h58 to 0h18 UT, of atmospheric parameters values given by the two methods (SA and FT) superimposed on the curves given by the radiosonde V471 launched the same night between 23h35 and 1h00 UT. In Fig. 1, six spatiotemporal cross-correlation peaks are visible. All these peaks were detected by both the SA and the FT methods. As noted, we have found almost all the turbulent layers showed by the radiosonde V471.

Values of $C_n^2(h_i)\Delta h_i$, which were calculated by the two optical methods, were divided by the corresponding vertical resolution $\Delta h = 500$ m, which is related to the altitude sampling. Since the search for turbulent layers was made with a step of 500 m between the ground and 3 km and a step of 1 km between 3 and 25 km, the radiosonde curves have been integrated using the same vertical sampling. Thus, in Figs 2(a) and 3(a), we presented the average of $C_n^2(h)$ over Δh_i which is defined as:

$$C_n^2(h_i) = \frac{1}{\Delta h_i} \int_{h_i}^{h_i + \Delta h_i} C_n^2(h) dh, \quad (5)$$

where $\Delta h_i = 500$ m between the ground and 3 km and $\Delta h_i = 1$ km between 3 and 25 km. In addition, altitude values found by

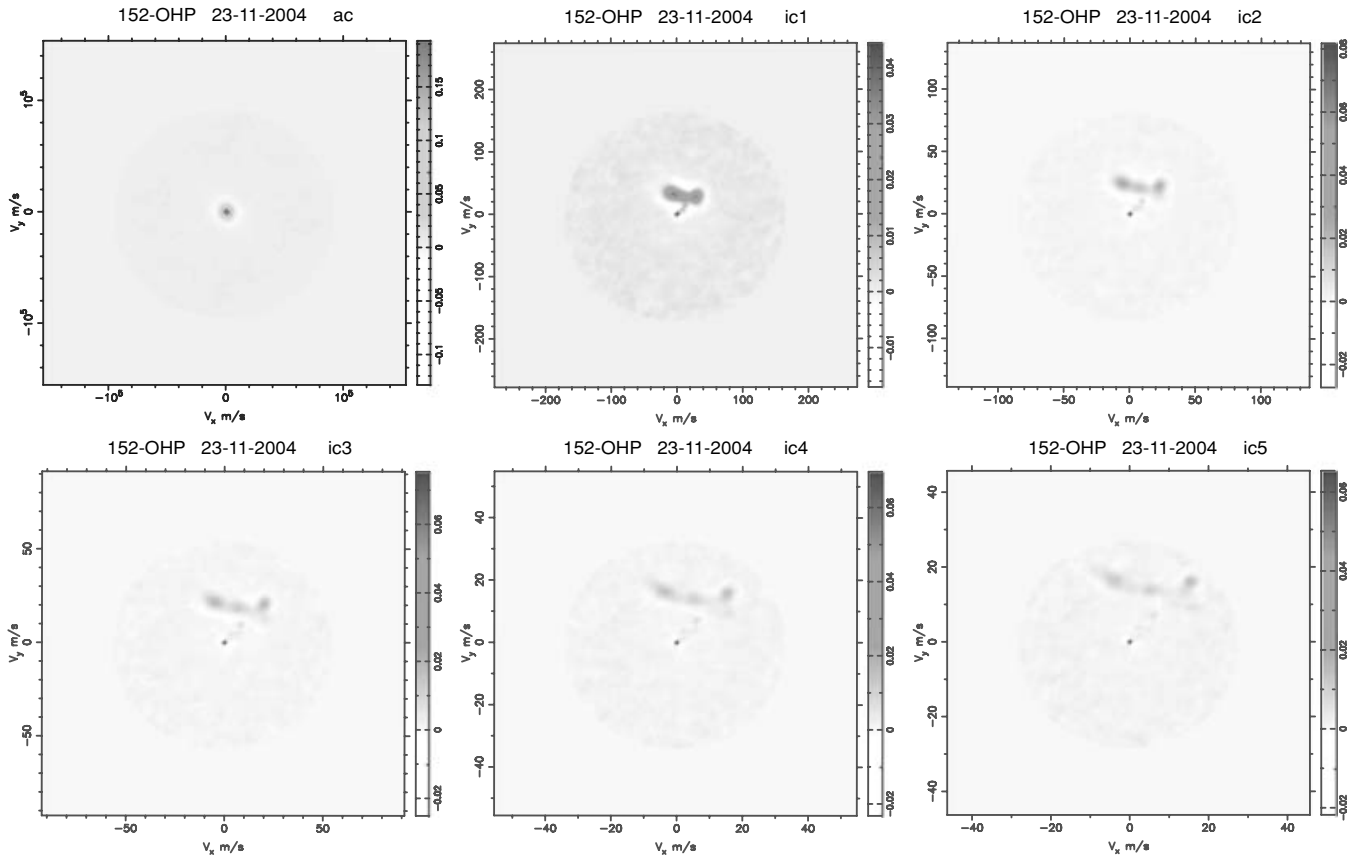


Figure 1. Example of a set of the experimental spatiotemporal cross-correlation functions obtained on the night of 2004 November 23 from 23h58 UT. The number of images used for the calculation of these functions is 2000. The observed single star was β Tauri. The analysis plane was at $h_{\text{sg}} = -1$ km. The exposure time was 1 ms. The grey-scale indicates the spatiotemporal cross-correlation function values. We can observe six visible peaks.

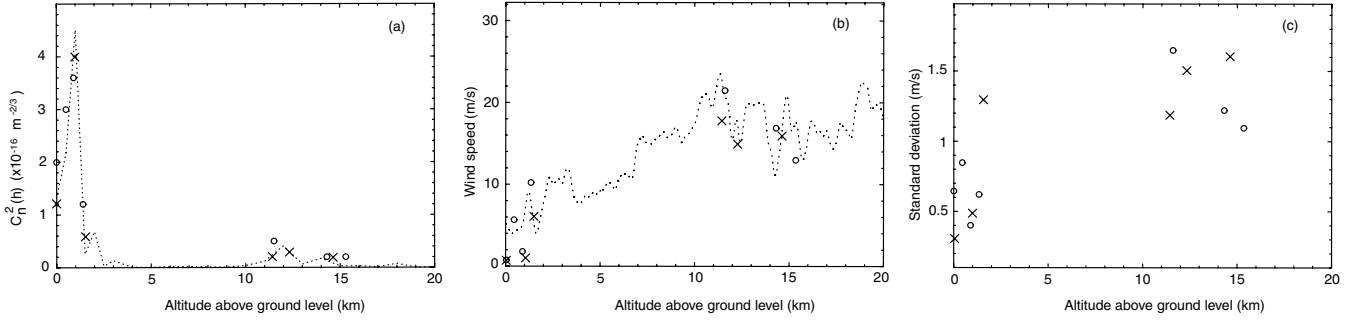


Figure 2. Average, from 23h58 to 0h18 UT, of atmospheric parameters values calculated with the SA method (circles) and the FT method (\times) using spatiotemporal cross-correlation functions ic3, ic4 and ic5. The observed single star was Alnath (β Tauri) and the analysis plane was situated at $h_{sg} = -1$ km. The dotted line represents radiosonde V471 results. Radiosonde $C_n^2(h)$ profile were integrated using the same vertical sampling as the two optical methods. Radiosonde $v(h)$ profile has been smoothed in order to have a visible presentation. With the SA method, we almost detected all the turbulent layers shown by the radiosonde except a weak one at 18 km.

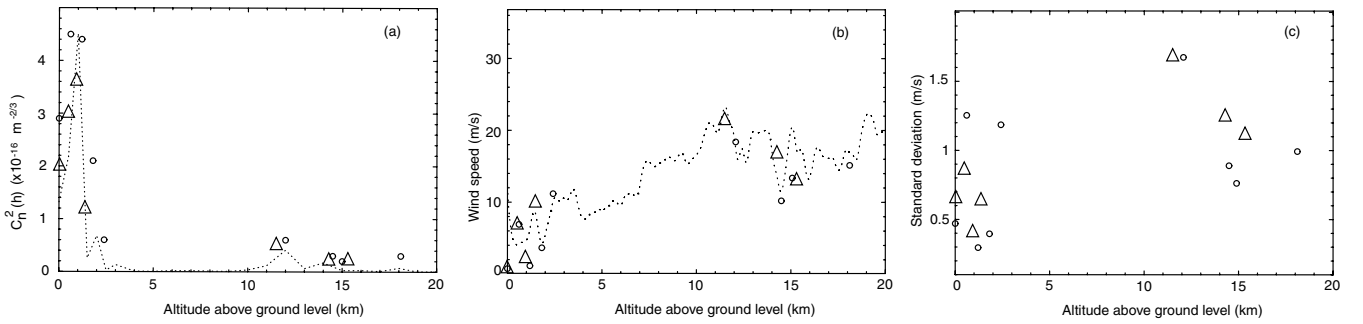


Figure 3. The results of the SA method obtained by using cross-correlations ic1–ic2 (circles) and cross-correlations ic3–ic4–ic5 (triangles) superimposed to the radiosonde V471 result (dotted line) on the night of 2004 November 23. The SA result is an average from 23h58 to 0h18 UT. The observed single star was β Tauri and the analysis plane was situated at $h_{sg} = -1$ km. A good correspondance is noted, in panels (a) and (b), between SA results and radiosonde results. In panel (c), we represented just our results because the radiosonde dose not give the standard deviation of horizontal wind fluctuations (σ_v).

Table 1. Values of turbulence strength $C_n^2(h_i)$ with the corresponding uncertainties (rms_i) and the wind speed modulus given by the SA method and the FT method using cross-correlations ic3–ic4–ic5. The SA method detected one more peak compared to the FT method. Taking into account the uncertainties, we can conclude that the two results are comparable.

SA				FT			
h_i (km)	$C_n^2(h_i)$ ($m^{-2/3} \times 10^{-16}$)	rms_i ($m^{-2/3} \times 10^{-16}$)	v_i ($m s^{-1}$)	h_i (km)	$C_n^2(h_i)$ ($m^{-2/3} \times 10^{-16}$)	rms_i ($m^{-2/3} \times 10^{-16}$)	v_i ($m s^{-1}$)
0	2	0.6	0.4	0	1.2	0.4	0.5
0.5	3	0.7	5.8				
0.9	3.6	0.5	1.9	1	4	1	1
1.4	1.2	0.4	10	1.5	0.6	0.2	6
11.5	0.5	0.1	21	11.4	0.2	0.05	18
				12.2	0.3	0.1	15
14.3	0.2	0.05	17	14.5	0.2	0.05	16
15.3	0.2	0.05	13				

the two optical methods were multiplied by $\sec(z)$, where z is the zenith angle of the observed single star. Fig. 2(b) shows the vertical profile of the wind speed modulus $v(h_i) = |v(h_i)|$. When $C_n^2(h_i)$ is non-zero, SA and FT methods give the corresponding values of the other atmospheric parameters, but if $C_n^2(h_i) = 0$, no information is available about wind speed and standard deviation of horizontal wind speed fluctuations, consequently, the corresponding values are not presented. Finally, Fig. 2(c) shows that the standard deviation of horizontal wind speed fluctuations (σ_v) given by the two optical methods are comparable. The radiosonde does not give this last parameter. However, while the FT method gave non-zero $C_n^2(h_i)$

values at six altitudes corresponding to the six visible spatiotemporal cross-correlation peaks, the SA method gave non-zero values at seven altitudes. This means that the SA method resolves sublayers which are too close to be detected by the FT method. The corresponding cross-correlation peaks are weak and not well visible in the cross-correlation functions.

Table 1 lists the atmospheric parameters values given by the two SA and FT methods. In this table, we presented altitudes h_i , turbulence strength $C_n^2(h_i)$, uncertainties rms_i on $C_n^2(h_i)$ values and wind speed modulus. The peak with a low speed, near the ground, may correspond to the turbulence inside the telescope dome (Avila,

Table 2. Values of turbulence strength $C_n^2(h_i)$ with the corresponding uncertainties (rms_i) and the wind speed modulus obtained by the SA method using cross-correlations ic3–ic4–ic5 (left part) and ic1–ic2 (right part). With cross-correlations ic1–ic2, we detected two more turbulent layers.

SA (ic3–ic4–ic5)				SA (ic1–ic2)			
h_i (km)	$C_n^2(h_i)$ ($m^{-2/3} \times 10^{-16}$)	rms_i ($m^{-2/3} \times 10^{-16}$)	v_i ($m s^{-1}$)	h_i (km)	$C_n^2(h_i)$ ($m^{-2/3} \times 10^{-16}$)	rms_i ($m^{-2/3} \times 10^{-16}$)	v_i ($m s^{-1}$)
0	2	0.6	0.4	0	2.9	0.7	0.4
0.5	3	0.7	5.8	0.6	4.5	1	6.8
0.9	3.6	0.5	1.9	1.2	4.4	0.5	1.
				1.8	2.1	0.6	3.8
1.4	1.2	0.4	10	2.4	0.6	0.15	11
11.5	0.5	0.1	21	12	0.6	0.28	18.5
14.3	0.2	0.05	17	14.5	0.3	0.05	10.2
15.3	0.2	0.05	13	15.	0.2	0.08	13.5
				18.1	0.3	0.04	15.2

Vernin & Sánchez 2001). Since the pixel size on the telescope pupil is $d_x = 0.02$ m, the corresponding wind speed resolution, which is related to the positions of the correlation peak centres, is $dx/\tau_3 = 0.89$ $m s^{-1}$ ($\tau_3 = 22.4$ ms).

4.2.2 Results extracted from cross-correlations ic1 and ic2

If we try to use the cross-correlation functions ic1 and ic2, where the correlation peaks are mixed, the first method (FT) is useless. But, the new SA method allows us to obtain the atmospheric parameters even if spatiotemporal cross-correlation peaks are not well separated. Fig. 3 shows the average of atmospheric parameters values given by the SA method on 2004 November 23, from 23h58 to 0h18 UT, and the result given by the radiosonde V471. We also presented the results obtained in the previous section with cross-correlations ic3–ic4–ic5. It is noted that our points are very close to the radiosonde curve. Fig. 3(c) shows the values of the standard deviation of horizontal wind speed fluctuations (σ_v). These values have the same order of magnitude as those found by Caccia & Vernin (1990) and by Habib et al. (2005). We should note that the radiosonde drift out of the Generalized Scidar range, which is why some differences may be noted between our results and those of the radiosonde.

Table 2 lists values of $C_n^2(h_i)$, with their uncertainties rms_i , and wind speed modulus obtained with the SA method. In this case, wind speed resolution is $dx/\tau_1 = 1.78$ $m s^{-1}$ ($\tau_1 = 11.2$ ms). At 18 km, for example, we have a new turbulent layer which was not detected by the SA and FT methods in the previous section (Fig. 2), this is because the corresponding spatiotemporal cross-correlation peak is weak for large values of τ as in ic3, ic4 and ic5.

To estimate the amount of the atmospheric turbulence taken into account, we represented in Fig. 4(a) the radial cut of the experimental auto-correlation function (ac) and the theoretical one that was calculated using the SA results. It is notable that the two curves are almost identical except in the centre where there is an additional peak corresponding to photons noise. The difference between these two curves is less than 3 per cent, which means that we have taken into account more than 97 per cent of the total amount of turbulence.

4.3 Temporal evolution

4.3.1 Temporal evolution of $\log[C_n^2(h, t)]$ and $v(h, t)$

With the SA method, we obtain an atmospheric parameter profile every 11.2 s which allows us to follow the temporal evolution of turbulence strength $C_n^2(h)$ and wind speed modulus. Fig. 5 shows

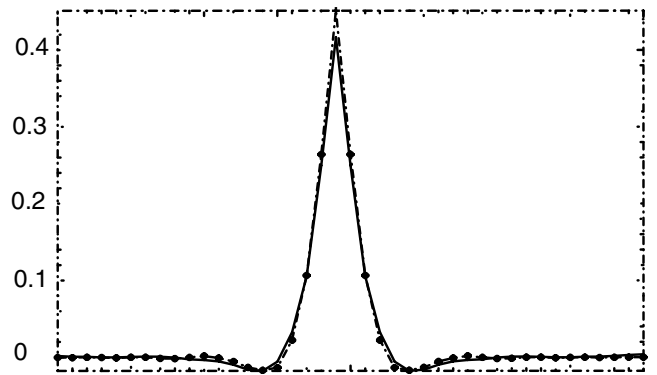


Figure 4. Radial cut of the experimental auto-correlation (dot–dashed line) and the auto-correlation built from the SA results (full line).

an example of $\log[C_n^2(h, t)]$ and $v(h, t)$ as functions of time and altitude obtained on the night of 2004 November 23 from 23h58 to 0h18 UT. The temporal sampling is one profile every 11.2 s. The single star observed was β Tauri. The analysis plane was located at $h_{sg} = -1$ km. The two profiles show the same turbulent layers since when $C_n^2(h)$ is 0, the wind speed modulus v is not calculated. Three turbulent layers are visible between the ground and 3 km, where turbulence is intense. The abrupt temporal variations are due to the turbulence intermittencies.

4.3.2 Parameters for adaptive optics

From $C_n^2(h)$ and $v(h)$ values, we are able to retrieve astrophysics parameters for adaptive optics: the seeing ε , the coherence time of the wavefront τ_{AO} and the isoplanatic angle θ_{AO} (Roddier, Gilli & Lund 1982a; Roddier, Gilli & Vernin 1982b). The seeing is

$$\varepsilon = \frac{\lambda}{r_0}, \quad (6)$$

where λ is the wavelength of the used light and r_0 is Fried's parameter defined as:

$$r_0 = \left[16.7 \lambda^{-2} \sum_i C_n^2(h_i) \Delta h_i \right]^{3/5}. \quad (7)$$

The coherence time of the wavefront τ_{AO} is

$$\tau_{AO} = 0.31 \frac{r_0}{v_{AO}}, \quad (8)$$

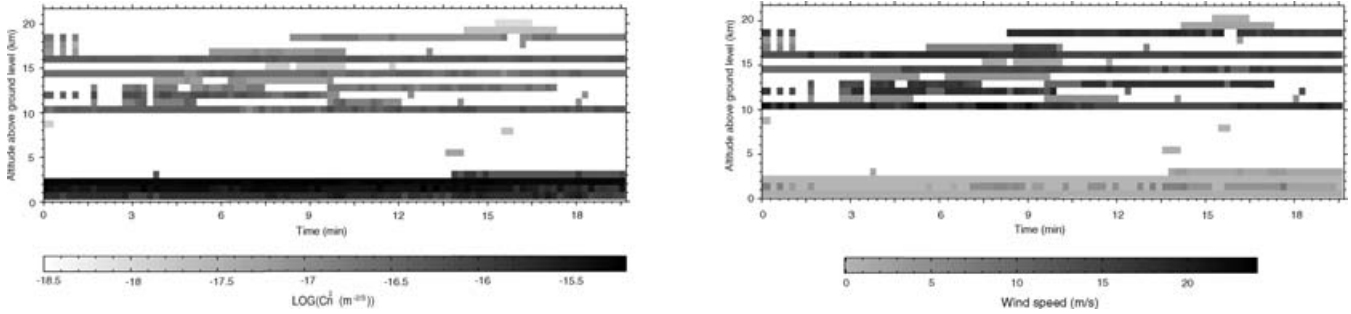


Figure 5. Example of temporal evolution, using cross-correlations ic1–ic2, of the vertical profiles of turbulence strength $\log [C_n^2(h, t)]$ and wind speed modulus $v(h, t)$ obtained on 2004 November 23 from 23h58 to 0h18 UT. The observed single star was β Tauri and the analysis plane was situated at $h_{\text{sg}} = -1$ km. The temporal sampling is one profile every 11.2 s. The grey-scale shows the values of $\log [C_n^2(h, t)]$ and $v(h, t)$. When $C_n^2(h) = 0$ (the white area), the wind speed is not calculated (the white area).

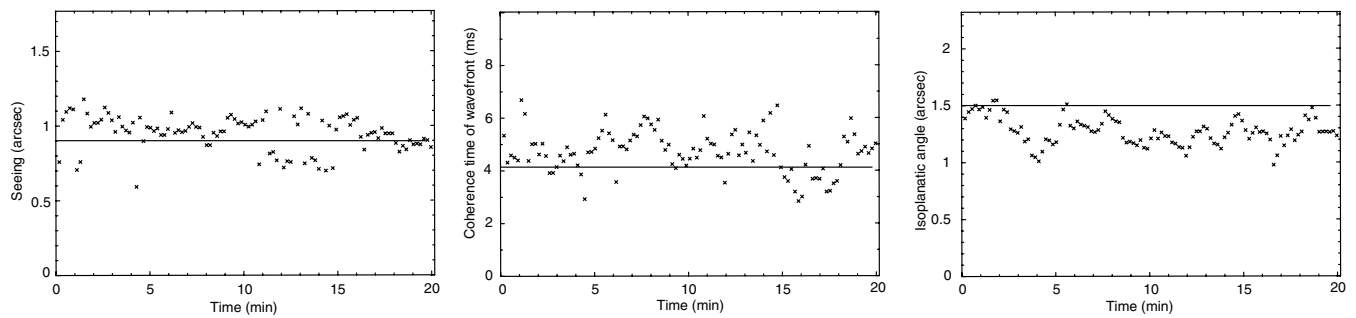


Figure 6. Temporal evolution of the seeing, the coherence time of the wavefront and the isoplanatic angle obtained from our results on the night of November 23 between 23h58 and 0h18 UT. In our calculations, we have not taken into account the turbulence inside the telescope dome. Horizontal lines present the radiosonde V471 values.

where the characteristic speed is defined as:

$$v_{\text{AO}} = \left[\frac{\sum_i |v(h_i)|^{5/3} C_n^2(h_i) \Delta h_i}{\sum_i C_n^2(h_i) \Delta h_i} \right]^{3/5}. \quad (9)$$

The isoplanatic angle θ_{AO} is

$$\theta_{\text{AO}} = 0.31 \frac{r_0}{h_{\text{AO}}}, \quad (10)$$

where the characteristic altitude h_{AO} is given by:

$$h_{\text{AO}} = \left[\frac{\sum_i h_i^{5/3} C_n^2(h_i) \Delta h_i}{\sum_i C_n^2(h_i) \Delta h_i} \right]^{3/5}. \quad (11)$$

Fig. 6 represents the temporal evolution of the seeing, the coherence time of the wavefront and the isoplanatic angle where the eventual dome turbulence was removed. Horizontal lines present the values of these three parameters calculated from the radiosonde V471 data which are: $\varepsilon = 0.9$ arcsec, $\theta_{\text{AO}} = 1.5$ arcsec and $\tau_{\text{AO}} = 4.1$ ms. As we can see in Fig. 6, these values are very close to the averages of the three parameters.

5 CONCLUSION

We presented a new method to retrieve simultaneously vertical profiles of turbulence strength, horizontal wind speed and the standard deviation of the horizontal wind speed fluctuations from the ground level up to 25 km or more. With this method, we are able to get atmospheric parameters from the spatiotemporal cross-correlation function of atmospheric speckles even if the cross-correlation peaks

are not separated from each other. The temporal sampling of the method, which depends on the camera and the computer features, is one profile every 11.2 s. From the turbulence strength and wind speed modulus values, it is possible to get the seeing, the isoplanatic angle and the coherence time of the wavefront which are very important in adaptive optics.

Comparison of the results with radiosonde data and FT technique (Habib et al. 2005) shows good agreement and demonstrates the efficiency of this method. Thus, we can conclude that this new method is validated and gives reliable results. Consequently, it is an adequate technique for high angular resolution astronomy.

However, in the case of high wind speeds, if some spatiotemporal cross-correlation peaks leave the pupil boundaries for the delay τ_2 , the SA method will not be able to extract the corresponding atmospheric parameters because it uses at least two spatiotemporal cross-correlation functions $C(\mathbf{r}, \tau_1)$ and $C(\mathbf{r}, \tau_2)$.

In our case, the lowest values of τ_1 and τ_2 are related to our CCD device, $\tau_1 = 5.6$ ms and $\tau_2 = 11.2$ ms. Let us assume that we use a 40-cm telescope. The maximum wind speed which can be detected is about 36 m s^{-1} , which does not occur frequently. Consequently, this method will allow us to bring to reality the mobile SCIDAR system using a small telescope diameter. This system will be useful for testing remote sites where no large telescope is available.

In addition, the result reported in this paper shows agreement between theory and experiment and confirms that the hypotheses we used in our study, which are: Taylor's hypothesis, small perturbations hypothesis, the Gaussian model of wind fluctuations and the statistical independence of turbulent layers, are well verified.

ACKNOWLEDGMENTS

Authors wish to thank all participants in OHP-2004 Gravity Wave campaign for providing balloons and Scidar data and many technical aspects. This mission was organized in collaboration with US Air Force Research Laboratory (contract F61775-02-C0002). This work was also financially supported by a France–Morocco international collaboration Programme, PICS.

REFERENCES

Azouit M., Vernin J., 2005, *Publ. Astron. Soc. Pac.*, 117, 563
 Avila R., Vernin J., Sánchez, 2001, *A&A*, 369, 364
 Caccia J.-L., Vernin J., 1990, *J. Geophys. Res.*, 95-D9, 683
 Caccia J.-L., Azouit M., Vernin J., 1987, *Appl. Opt.*, 26, 1288
 Habib A., Vernin J., Benkhaldoun Z., 2005, *C.R.A.S Paris, Physique*, 6, 385

Kirkpatrick S., Gelett C. D. Jr., Vecchi M. P., 1983, *Sci*, 220, 671
 Press W. H., Flannery B. P., Teukolsky S. A., Vetterling W. T., *Numerical Recipes In Fortran 77: The Art of Scientific Computing*. Cambridge Univ. Press, Cambridge
 Rocca A., Roddier F., Vernin J., 1974, *J. Opt. Soc. Am.*, 64, 1000
 Roddier F., 1981, *E.WOLF Ed.*, XIX-ed. (North-Holland, Amsterdam), 19, 281
 Roddier F., Gilli J. M., Lund G., 1982a, *J. Opt. Paris*, 13, 263
 Roddier F., Gilli J. M., Vernin J., 1982b, *J. Opt. Paris*, 13, 63
 Tatarski V.I., 1961, Dover, New York
 Van Laarhoven P. J. M., Aarts E. H. L., 1987, *Theory and Applications of Simulated Annealing*. Kluwer Academic Publishers, London
 Vernin J., Azouit M., 1983a, *J. Opt. Paris*, 14, 5
 Vernin J., Roddier F., 1973, *J. Opt. Soc. Am.*, 63, 270

This paper has been typeset from a \TeX/L\TeX file prepared by the author.